Earth and Planetary Science Letters 498 (2018) 27–37

Contents lists available at ScienceDirect

Earth and Planetary Science Letters

www.elsevier.com/locate/epsl

# Effect of dehydrogenation on the electrical conductivity of Fe-bearing amphibole: Implications for high conductivity anomalies in subduction zones and continental crust

Haiying Hu [a,b], Lidong Dai [a,*], Heping Li [a], Wenqing Sun [a,c], Baosheng Li [b]

[a] Key Laboratory for High-Temperature and High-Pressure Study of the Earth's Interior, Institute of Geochemistry, Chinese Academy of Sciences, Guiyang, Guizhou, 550002, China
[b] Mineral Physics Institute, Stony Brook University, Stony Brook, NY 11794, USA
[c] University of Chinese Academy of Sciences, Beijing 100039, China

ARTICLE INFO

*Article history:*
Received 17 January 2018
Received in revised form 31 May 2018
Accepted 4 June 2018
Available online xxxx
Editor: J. Brodholt

*Keywords:*
Fe-bearing amphibole
electrical conductivity
dehydrogenation
highly conductive anomalies
continental mid-crust and subduction zones

ABSTRACT

Magnetotelluric measurements reveal the presence of high conductivity anomalies (up to ~1 S/m) in both the forearc and backarc regions of subduction zones as well as the continental middle–lower crust. Such anomalies are commonly interpreted as a consequence of aqueous fluid released from the dehydration of hydrous minerals. Amphibole is an important constituent of the continental mid-crust and a major hydrous phase in subduction zones, such that its dehydration at high temperature has been suggested to provide a significant source of aqueous fluid. We performed electrical conductivity measurements of a natural Fe-bearing amphibole at 623–1173 K and 0.5–2.0 GPa using a multi-anvil apparatus and an impedance spectroscopy. Our results show that pressure has a very weak effect on conductivity compared with temperature. An abrupt variation of the impedance semicircular arc followed by a remarkable increase of electrical conductivity is observed at temperature of 843 ± 20 K. However, the enhancement in conductivity is not attributed to conductive aqueous fluid but rather to amphibole oxidation–dehydrogenation, as confirmed by infrared spectroscopy and optical microscopy observations. A slight decrease in activation enthalpy from ~0.80 eV to ~0.70 eV suggests that the conduction mechanism does not change before and after dehydrogenation, and small polaron conduction (electron holes hopping between $Fe^{2+}$ and $Fe^{3+}$) is considered to dominate the conductivity of amphibole over the entire temperature range. Although amphibole dehydrogenation at high temperature cannot serve as a principal source of aqueous fluid, the enhanced electrical conductivity of amphibole after dehydrogenation is sufficient to account for the high conductivity anomalies observed in slab–mantle wedge interfaces and the continental lowermost mid-crust, particularly in local regions with high heat flow.



## 1. Introduction

Magnetotelluric (MT) sounding results reveal that high conductivity anomalies are widely present both in the continental mid-crust as well as backarc and forearc regions of subduction zones, characterized by conductivity values of 0.01–1 S/m (Leibecker et al., 2002; Wannamaker et al., 2009; Worzewski et al., 2011; Evans et al., 2014; McGary et al., 2014). These anomalies are generally explained by the presence of NaCl-bearing aqueous fluids (Hyndman and Shearer, 1989; Sinmyo and Keppler, 2017), partial melts (Schilling et al., 1997; Glover et al., 2000), and interconnected highly conductive minerals such as graphite film (Glover and Vine, 1994), Fe/Ti-oxides, or sulfides (Duba et al., 1994; Kawano et al., 2012). Among these explanations, aqueous fluid is usually considered to be the most likely cause of the observed high-conductivity anomalies because fluids are formed during heating of the continental mid-crust by underlying mantle plumes or released from dehydration of hydrous phases in subduction zones (Wannamaker et al., 2009; Worzewski et al., 2011). However, the non-unique inverse problem of magnetotellurics hardly provides an accurate interpretation of MT field data, while laboratory-based electrical conductivity measurements of geomaterials can significantly constrain the geophysical observations. Recent experimental measurements of the conductivity on hydrous minerals indicate that dehydration provides a crucial source of

* Corresponding author.
*E-mail address:* dailidong@vip.gyig.ac.cn (L. Dai).

https://doi.org/10.1016/j.epsl.2018.06.003
0012-821X/

**Table 1**
The chemical composition of sample before electrical conductivity measurement (wt.%).

| Sample | $SiO_2$ | $Al_2O_3$ | CaO | MgO | $TiO_2$ | MnO | FeO | $Na_2O$ | Total |
|---|---|---|---|---|---|---|---|---|---|
| Am | 50.56 | 3.66 | 20.43 | 14.29 | 1.00 | 0.21 | 8.16 | 0.38 | 98.69 |

aqueous fluid that may be responsible for the high conductivity anomalies, particularly in subduction zones where a large amount of hydrous minerals are stable at a range of depths (Manthilake et al., 2015, 2016; Chen et al., 2017; Hu et al., 2017).

According to the generalized mineralogical composition model of continental crust given in Christensen and Mooney (1995), amphibole content reaches up to 35–40 vol.% at depths of 15–30 km, corresponding to the average continental mid-crust. Similarly, amphibole is an important water carrier with abundances up to 50 vol.% in epidote-amphibolite and amphibolite facies in subduction zones (Schmidt and Poli, 1998). Consequently, the dehydration of amphibole containing 2.1 wt.% $H_2O$ may make a significant contribution to the source of aqueous fluid, both in the continental mid-crust and subduction zones. However, numerous crystallographic studies on Fe-bearing amphibole have demonstrated that extensive dehydrogenation takes place at high temperature ($T$), simultaneously associated with the oxidation of $Fe^{2+}$ into $Fe^{3+}$, such that $H_2$ is released instead of molecular water (Phillips et al., 1988; Della Ventura et al., 2017). Thus, the electrical conductivity and conduction behavior of amphibole under relevant pressure ($P$) and $T$ conditions are of critical importance for understanding the origin of highly conductive anomalies observed in continental crust and subduction zones.

The electrical conductivity of amphibole or amphibolite has attracted considerable attention in recent decades. Most previous data were obtained at low $T$ (<923 K) (Tolland, 1973; Zhou et al., 2011), while a small number of studies were performed outside the amphibole stability field (Glover and Vine, 1994, 1995; Schmidbauer et al., 2000; Wang et al., 2012), and some reported the occurrence of dehydration or oxidation–dehydrogenation processes inferred from the dramatic variation of conductivity and activation energy when sample was heated to the temperature of dehydrogenation ($T_D$). Schmidbauer et al. (2000) reported that, above 873 K, conduction processes are characterized by a low activation energy (<1.0 eV) and suggested the occurrence of dehydrogenation or some sort of initial amphibole decomposition without the influence of $H_2$. In contrast, Wang et al. (2012) showed that at $T$ above ~800 K, where dehydration occurs, the conductivity abruptly increases and activation enthalpies are anomalous high (up to 3.32–3.94 eV) but the conduction behavior remains unclear. The widely inconsistent activation energies and ambiguity regarding the conduction mechanism reported in previous studies demands further investigation to meticulously measure the conductivity of amphibole under well-controlled $P$–$T$ conditions to constrain the influence of oxidation–dehydrogenation on conductivity and the corresponding conduction behavior.

In this study, impedance spectroscopy measurements were performed over the $P$–$T$ range of 623–1173 K and 0.5–2.0 GPa in a multi-anvil apparatus to investigate the effect of oxidation–dehydrogenation on the conductivity of Fe-bearing amphibole. We discuss the conduction mechanisms before and after amphibole dehydrogenation in detail according to Arrhenius parameters (e.g., activation enthalpy) characterizing conduction behavior, and the probable effect of Fe content on conductivity based on the present and previous data. Finally, a conductivity–depth profile from the amphibole results is established, and principal implications for the origin of the anomalously high conductivity observed in the continental mid-crust and subduction zones are comprehensively evaluated.

## 2. Experimental methods

### 2.1. Sample preparation

The starting materials were dark green, prism-shaped amphibole single crystals from Sichuan province, China. The samples contain very small amounts of accessory minerals (e.g., plagioclase, quartz, and rutile) and appear as isolated pocket shapes in the amphibole matrix, as observed by the scanning electron microscope (SEM) analysis, and would therefore have a negligible influence on the bulk conductivity of amphibole. Sample chemical composition was determined using an electron microprobe analyzer (EPMA-1600) operated at the State Key Laboratory of Ore-Deposit Geochemistry, Institute of Geochemistry, Chinese Academy of Sciences (CAS). Analytical results are listed in Table 1. Amphibole crystals were cut parallel to the $c$-axis using a diamond slicer and polished into cylindrical shapes with a diameter of 6.0 mm and lengths of 3.0–6.0 mm. Samples were then cleaned successively in acetone and ethanol using an ultrasonic cleaner and kept dry in a muffle furnace at 423 K until the sample was assembled.

### 2.2. In situ electrical conductivity measurements

Electrical conductivity experiments were performed at the Key Laboratory of High-Temperature and High-Pressure Study of the Earth's Interior, Institute of Geochemistry, CAS, China and at the Mineral Physics Institute (MPI), Department of Geosciences, Stony Brook University, USA. Since oxygen fugacity in subduction zones is estimated to be several log units more oxidized than the surrounding mantle (relative to FMQ) (McCammon et al., 2004), two symmetric Ni electrodes and a Ni foil shielding case were chosen to fix oxygen fugacity close to the nickel–nickel oxide (NNO) buffer. The sample was placed in an $Al_2O_3$ capsule and sandwiched by the Ni electrodes separately connected with two nickel–aluminum ($Ni_{97}Al_3$) wires that were insulated from the stainless steel furnace by $Al_2O_3$ insulation sleeve. A cylindrical MgO sleeve was used outside the $Al_2O_3$ capsule to maintain thermal insulation. The Ni foil shielding case was grounded by a wire between the MgO and $Al_2O_3$ capsule to shield external electromagnetic disturbance and minimize the temperature gradient across the sample. The heater was constructed of three layers of stainless steel sheets that were installed inside the pyrophyllite pressure medium. A welded $Ni_{90}Cr_{10}$–$Ni_{97}Al_3$ thermocouple was placed in direct contact with the middle of the sample to monitor the temperature. The temperature gradient was roughly estimated to 5 K in this sample cell. The cell design for conductivity measurement resembles that in our previous work (Dai et al., 2016; Hu et al., 2017). After the completion of sample assembly, it was stored in muffle furnace at 423 K until the electrical conductivity measurement in order to avoid moisture.

High pressures and temperatures were generated using a YJ-3000t multi-anvil apparatus at the Institute of Geochemistry, CAS. Complex impedance spectra of the samples were measured over 623–1173 K and 0.5–2.0 GPa by a Solartron-1260 Impedance/Gain-Phase analyzer. The 1 V amplitude of the applied voltage for the alternating current over a frequency range of $10^{-1}$–$10^6$ Hz was adopted to determine the sample resistance. Two sets of conductivity measurements were initially performed separately to observe both the temperature of oxidation–dehydrogenation, $T_D$ and the time required to reach a steady resistance

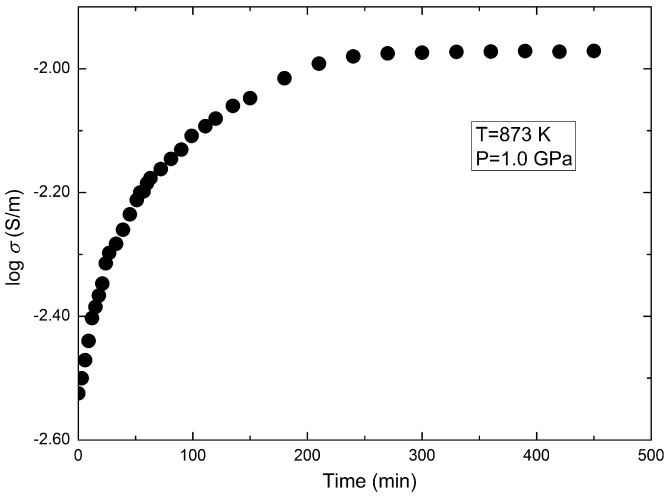


**Fig. 1.** The electrical conductivity of sample as a function of time at 873 K and 1.0 GPa during dehydrogenation process.

at $T_D$. A continuous heating–cooling cycle mode was employed: when pressure was increased to a designed value, impedance spectra were collected in the first heating–cooling cycle below 923 K at 50 K steps to attain the reproducible conductance within the amphibole stability field. After that, impedance spectra were then collected continuously in several heating–cooling cycles at 623–1173 K with the same step until reproducibility of resistance values was achieved. Variation of impedance spectra and conductivity with temperature indicate that the onset of oxidation–dehydrogenation in amphibole occurs at $843 \pm 20$ K. A subsequent individual conductivity measurement was carried out at 873 K to monitor the time required to achieve steady state from the onset to completion of sample dehydrogenation. The plot of electrical conductivity versus elapsed time shown in Fig. 1 indicates that at least 200 min are required to attain a steady impedance value at 873 K.

In light of the results above, the electrical conductivity measurements of amphibole at different $P$ (0.5–2.0 GPa) were performed by a discontinuous heating–cooling mode. After the sample was compressed to the desired pressure, the first heating–cooling cycle was repeated below 923 K in the same manner as in the continuous mode. The sample was then heated to 873 K and held for 200 min. While the resistance reproducibility was confirmed at this $T$. The sample was then heated again to 1173 K. The subsequent heating and cooling cycles were repeated in the $T$ range of 623–1173 K to verify reproducibility after sample dehydrogenation. The temperature was continuously varied at each 50 K interval and impedance spectra were achieved accordingly. After completion of the conductivity measurements, samples were quenched and decompressed to ambient pressure. The experimental conditions are listed in Table 2.

### 2.3. Post-experiment sample characterization

Recovered samples from the continuous and discontinuous heating–cooling cycles were polished for micro-textural analyses and phase identification. Analyses were performed by virtue of the optical microscope and scanning electron microscope (JSM-7800F) with a typical acceleration voltage and beam current of 20 kV and 2.0 nA, respectively. The images are displayed in Fig. 2. Microfracture and cleavage were observed to be more abundant in samples from the discontinuous mode measurements compared to those made using the continuous mode. No new phases were detected except that the sample color varied from dark green to brown and fractures were observed.

The water contents of samples before and after conductivity measurements were analyzed using a Fourier transform vacuum infrared (FTIR) spectrometer (Vertex-70V, Hyperion-1000 infrared microscope). Samples for IR analysis were polished to a thickness of less than 100 μm. The IR absorption of samples was measured by unpolarized radiation with mid-IR light sources, a $CaF_2$ beam splitter, and an MCT detector with a $100 \times 100$ μm aperture. Spectra were collected from the total absorbance of OH between wavenumbers of 3000–3800 $cm^{-1}$ with 512 scans accumulated for each sample. Several main absorption bands were present prior to the conductivity measurements (Fig. S1 in supplementary material), similar to previous high-$T$ studies on synthetic and single crystals with the principal OH-stretching region between 3600–3800 $cm^{-1}$ (Della Ventura et al., 2017). The main band intensity dramatically decreased after conductivity measurements, which confirmed the occurrence of dehydrogenation and the loss of hydrogen during the high $P$–$T$ experiments.

## 3. Results

Two sets of typical complex impedance spectra measured from the amphibole samples in the continuous and discontinuous heating–cooling cycles are shown in Fig. 3. At $T$ below 873 K (i.e. before dehydrogenation), all the measured impedance spectra display an almost ideal semicircle centered on the real axis ($Z'$) in the high frequency range and a small low-frequency tail. The semicircular arc represents the bulk conduction of the single crystal sample, and the tail in the low frequency regime is characteristic of electrical processes occurring at electrode–sample interface and is unrelated to the electrical properties of the sample (Roberts and Tyburczy, 1991), thus it was precluded in the fitting process of impedance spectra. For the continuous mode at $T \geq 873$ K (Fig. 3a(2)), however, the impedance arcs show the presence of an induction loop in the low-frequency regimes with a part of the positive imaginary axis $Z''$, which is generally attributed to chemical reaction at the sample–electrode interface (Macdonald, 1978). We hypothesize that the appearance of induction loops at high $T$ reflects the occurrence of oxidation–dehydrogenation processes within the sample. The similar behavior has also been reported

**Table 2**
Experimental conditions and the Arrhenius fitting parameters before and after complete dehydration of sample in this study and previous results.

| Run no. | $P$ (GPa) | $T_1$ before DHY | $T_2$ after DHY | $\sigma_{01}$ (S/m) | $\Delta H_1$ (eV) | $\sigma_{02}$ (S/m) | $\Delta H_2$ (eV) | Refs. |
|---|---|---|---|---|---|---|---|---|
| Am2101 | 0.5 | 623–873 | 923–1173 | 162 | 0.81 | 154 | 0.70 | This study |
| Am2105 | 1.0 | 623–873 | 923–1173 | 111 | 0.79 | 82 | 0.67 | |
| Am2112 | 1.5 | 623–873 | 923–1173 | 187 | 0.83 | 69 | 0.67 | |
| Am2117 | 2.0 | 623–873 | 923–1173 | 120 | 0.81 | 75 | 0.68 | |
| hornblendite | 0.5–1.0 | 373–800 | 800–900 | 37 | 0.68 | – | 3.56 | WGYK12 |
| amphibolite | 1.0 | 523–973 | – | 53 | 0.71–0.75 | – | – | ZFLX11 |
| calcic amphiboles | 0 | 573–873 | 573–1058 | – | 0.73 | – | 0.62 | SKFH00 |

References: WGYK12: Wang et al. (2012); ZFLX11: Zhou et al. (2011); SKFH00: Schmidbauer et al. (2000).
Abbreviation: DHY, dehydrogenation.

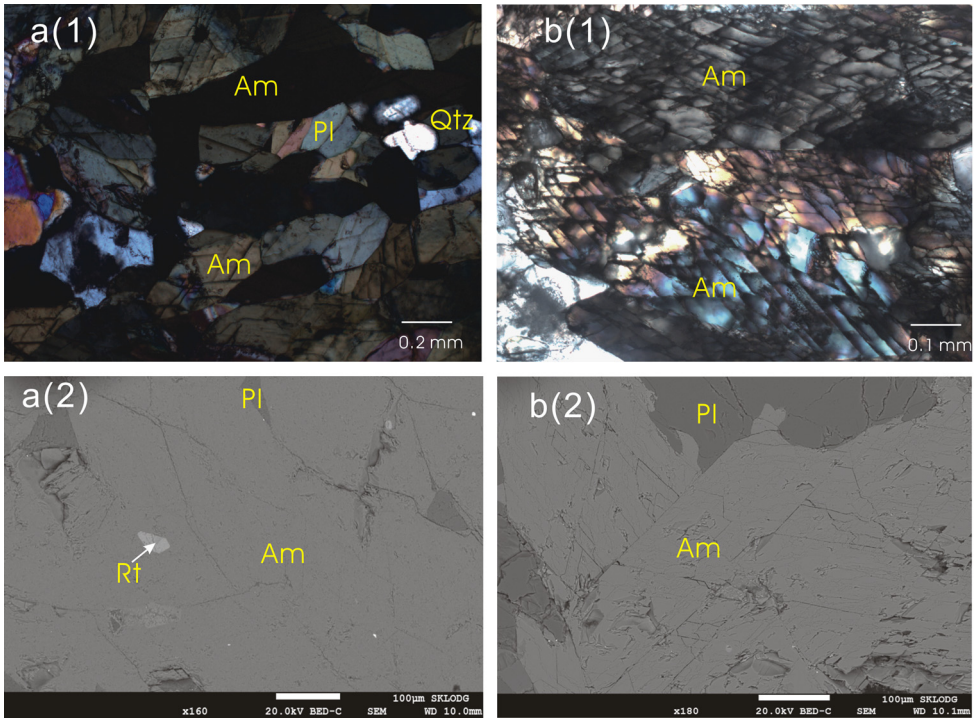


**Fig. 2.** The images of (a) optical and (b) scanning electron microscope for the samples after conductivity measurements in the continuous (left side) and discontinuous (right side) heating–cooling cycle modes, respectively. Abbreviations: Am, amphibole; Pl, plagioclase; Qtz, quartz; Rt, rulite.

for other hydrous minerals (e.g., talc, chlorite, and epidote) during dehydration (Wang and Karato, 2013; Manthilake et al., 2016; Hu et al., 2017). In contrast, after the sample maintained at 873 K for an extended time, impedance spectra collected above 873 K (Fig. 3b(2)) demonstrate a shape very similar to that measured below 873 K: a grain interior impedance arc and low-frequency tail. It is likely that the sample has reached equilibrium status, and the dehydrogenation reaction has possibly been completed according to the observation of FTIR. Sample resistance was determined by fitting impedance semi-circle arcs using an equivalent circuit consisting of a parallel resistor ($R$) and capacitor ($C$); the low-frequency tails representing the electrical processes at the sample–electrode interface were excluded during this fitting process.

The sample conductivity can be calculated from the resistance and a geometric factor according to $\sigma = L/SR$, where $L/S$, the geometric factor, is the sample length to electrode area ratio, and $R$ is the resistance of sample obtained by fitting the impedance spectra to an equivalent parallel circuit consisting of a resistor and a capacitor. Experimental errors mainly include the (1) fitting error of impedance arcs that are no more than 5%; (2) uncertainty from the precision of $T$ measurement ($\pm 5$ K) due to the thermal gradient along the length of sample cell; (3) Errors from geometric distortion can be almost negligible. Firstly, the sample dimension in this study was designed to be as large as possible so as to reduce or eliminate the effect of geometric change on conductivity. Besides, the sample geometry was essentially well preserved by measuring the sample dimension after conductivity measurements (Fig. S2 in supplementary material); (4) pressure uncertainty in sample cell was less than 0.1 GPa according to the previous pressure calibration in YJ-3000t multi-anvil apparatus from Shan et al. (2007). In summary, the total uncertainty of the final conductivity is estimated to be less than 10%.

The conductivities of Fe-bearing amphibole measured in the two different heating–cooling modes are shown in Fig. 4. At $T <$ 873 K, the conductivity demonstrates good reproducibility in both modes and the logarithmic conductivity increases with temperature. Once sample was heated above 873 K, electrical conductivity increases moderately with temperature and a distinct change of slope is observed around 873 K (Fig. 4a). For subsequent heating and cooling cycles, the electrical conductivities at $T > 873$ K fluctuates slightly, which likely arises from the non-equilibrium in the sample due to the incompletion of the oxidation–dehydrogenation. Previous experimental studies report that the dehydrogenation temperature, $T_D$, ranges between ~773 and 1073 K depending on several factors including the heating conditions of equilibrium or non-equilibrium, amphibole composition, sample shape (e.g., bulk or fibrous), and crystalline morphology (e.g., single crystal or powder) (Schmidbauer et al., 2000; Zema et al., 2012; Della Ventura et al., 2017). A distinct variation of the conductivity and FTIR observations verify the $T_D$ in this study at $843 \pm 20$ K. In the discontinuous heating–cooling modes, the conductivity was well reproducible after the sample was kept at 873 K for more than 200 min (Fig. 4b), and increases by ~0.5 log units after dehydrogenation.

Electrical conductivities measured in this study exhibit a linear relationship with temperature both before and after dehydrogenation, and can therefore be expressed by the Arrhenius equation;

$$\sigma = \sigma_0 \exp\left(\frac{-\Delta H}{kT}\right), \quad (1)$$

where $\sigma_0$ is a pre-exponential factor (S/m), $k$ is the Boltzmann constant (eV/K), and $\Delta H$ is the activation enthalpy for conduction (eV). Conductivity data obtained before and after dehydrogenation were fitted separately by Eq. (1), and the fitting parameters are summarized in Table 2. Fig. 5 shows the electrical conductivity of amphibole before and after dehydrogenation at 0.5–2.0 GPa. The temperature dependence of conductivities behaves similarly at varying pressure. At low $T$ (i.e., prior to dehydrogenation), the influence of pressure on conductivity almost can be negligible. After sample dehydrogenation, the electrical conductivity shows a weak negative pressure dependence that is far smaller than that of temperature. Additionally, activation enthalpy and the pre-exponential factor are also insensitive to the change of pressure, as listed in

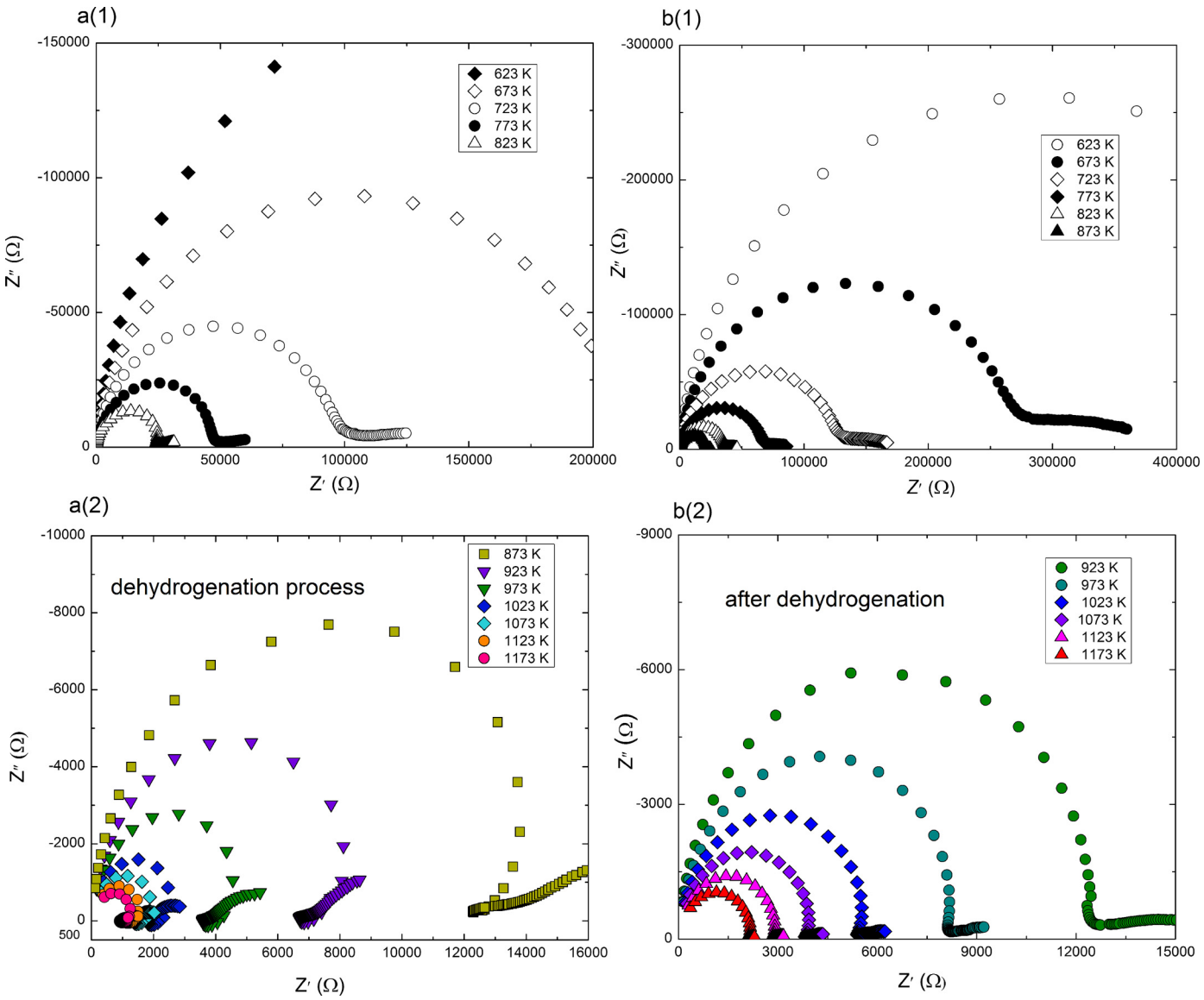


**Fig. 3.** Complex impedance spectra of Fe-bearing amphibole measured in the continuous (left) and discontinuous (right side) heating−cooling cycle modes, respectively. At temperatures below 923 K, all the complex impedance spectra shown in a(1) and b(1) exhibited a single impedance arc in high frequency regime plus a tail in the low frequency range for both of the heating modes. The impedance arcs measured by the continuous mode shown in a(2) indicate inductive loops in the low frequency regime at $T \geq 873$, reflecting the likely occurrence of an oxidation−dehydrogenation reaction, whereas the impedance arcs shown in b(2) are similar to those before dehydrogenation implying the probable completion of dehydrogenation reaction. An equivalent circuit of a single RC/CPE in parallel is used to fit these impedances arcs measured in the discontinuous modes.

Table 2. The pressure effect on electrical conductivity is therefore not taken into account in the discussion below. Nevertheless, $\Delta H$ values obtained before dehydrogenation are slightly higher (0.79–0.83 eV) than those obtained after dehydrogenation (approximately 0.70 eV). The small change in activation energy is related to the conduction mechanism of amphibole that is discussed in detail below.

## 4. Discussion

### 4.1. Conduction mechanism

Owing to the presence of two linear slopes in the Arrhenius plot before and after dehydrogenation, there are probably two different thermally activated conduction mechanism respectively controlling the conductivity, whereas the very small variation in activation energy at the two stages more likely arises from the tiny adjustment of crystal structure rather than the change of conduction mechanism. It is assumed that only one type of charge carriers dominates the electrical conductivity in whole experimental process. Ionic conduction generally occurs at relatively high $T$ and is characterized by a high activation energy (>2 eV); hence it is impossible to be the dominant charge migration mechanism due to the lower $\Delta H$ values (<1.0 eV) achieved by this study. Proton (H) conduction is commonly proposed to be the dominant conduction mechanism in hydrous minerals at low $T$ due to its small ionic radius and high mobility of H, and $\Delta H$ values are relatively low (<1 eV), such as 0.56–0.72 eV for brucite (Guo and Yoshino, 2014), 0.59–0.67 eV for talc, 0.68–0.74 eV for serpentinite (Guo et al., 2011), and 0.64–0.67 eV for epidote (Hu et al., 2017). Although activation enthalpy values in this study are very close to that for proton conduction, the smaller values (∼0.70 eV) determined at higher temperature after dehydrogenation imply that H is unlikely to control the bulk conductivity over the full temperature range because proton conduction is generally the dominant conduction mechanism at relatively low temperatures.

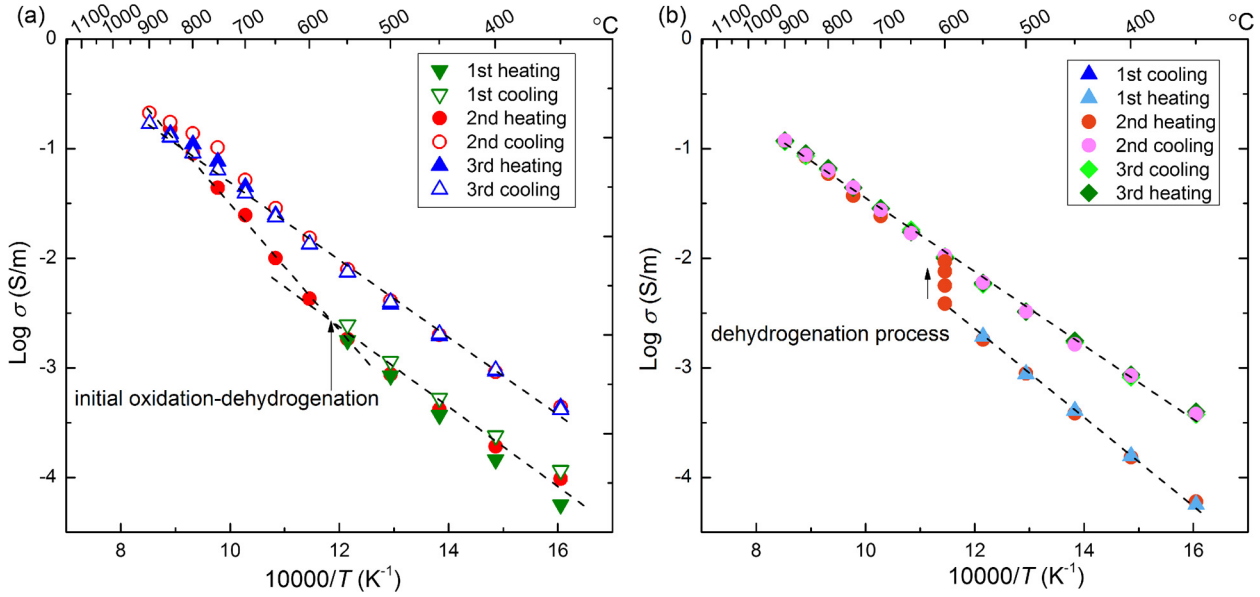


**Fig. 4.** Electrical conductivity of Fe-bearing amphibole as a function of reciprocal temperature in different repeated heating−cooling modes. (a) In the continuous mode, the remarkable change of slope of conductivity versus temperature occurs at around 843 K, and the electrical conductivities in the high temperature range (923–1173 K) exhibit a slight fluctuation where the dehydrogenation reaction occurs. (b) In the discontinuous mode, a continuous increase of conductivity is observed in the 2nd heating cycle when sample was kept at 873 K. After dehydrogenation in sample, the electrical conductivities are reproducible well in the 3rd heating–cooling cycle. The dashed lines denote the best fitting results by Equation (1).

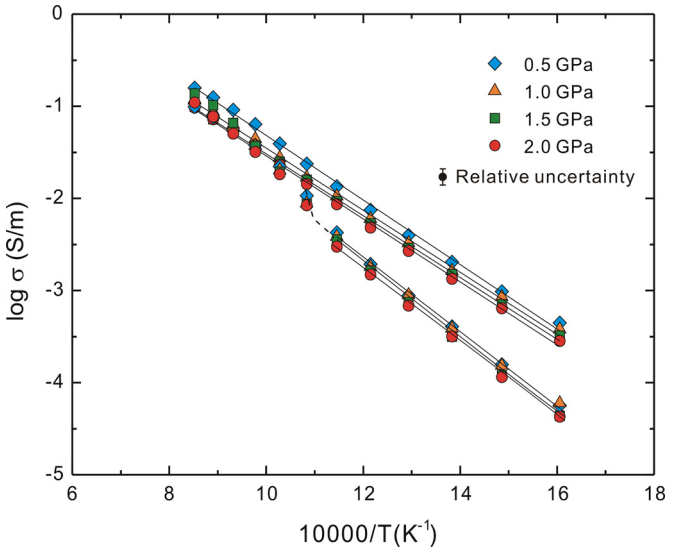


**Fig. 5.** Logarithm of electrical conductivity versus reciprocal temperature for Fe-bearing amphibole at variable confining pressures of 0.5–2.0 GPa. The solid lines indicate the fitting results of electrical conductivity by Equation (1). Pressure has a very small influence on the measured electrical conductivity of the amphibole, and even overlap at low temperature before dehydrogenation. The error bar is the assumed 10% relative uncertainty.

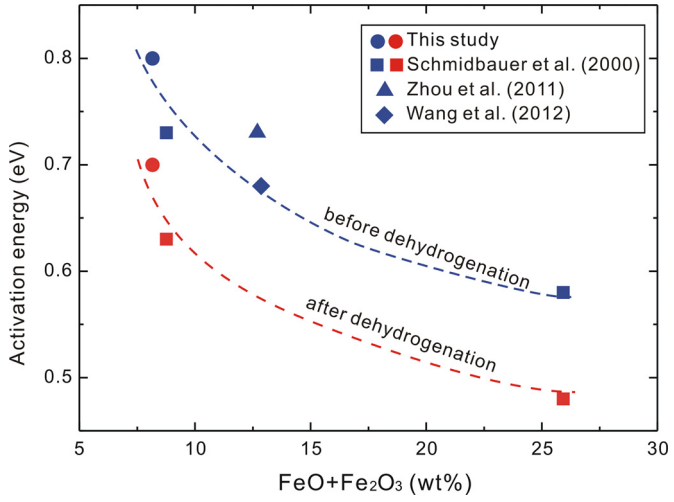


**Fig. 6.** Activation enthalpies for electrical conductivity in amphibole and amphibolite from present and previous studies. The dark blue and red symbols denote the activation enthalpies obtained before and after dehydrogenation, respectively, and correspondingly the blue and red dashed lines indicate their respective trend of activation enthalpies with total iron content. (For interpretation of the colors in the figure(s), the reader is referred to the web version of this article.)

In contrast, hopping (small polaron) conduction, which occurs through the electron transfer between ferrous and ferric ions, is considered the dominant charge transport mechanism in Fe-bearing silicate minerals including nominally hydrous minerals such as pyrophyllite (Hicks and Secco, 1997) and serpentine (Reynard et al., 2011). Reynard et al. (2011) showed that the electrical conductivity of serpentine is dependent on Fe concentration with reported $\Delta H$ values of ~1.3 eV. Although the $\Delta H$ values obtained here from Fe-bearing amphibole are slightly lower than those reported for other Fe-bearing hydrous minerals, small polaron conduction is likely to be the dominant charge transport mechanism because the activation energy for small polaron conduction spans a wide range of values in light of previous experimental results of Fe-bearing nominally hydrous minerals (Yoshino et al., 2012; Zhang and Yoshino, 2016).

Previous studies on Fe-bearing amphibole reveal that charge transport occurs mainly through electron hopping between $Fe^{2+}$ and $Fe^{3+}$. Correspondingly, the $\Delta H$ activation enthalpies are relatively low (<1.0 eV) both before and after dehydrogenation (Fig. 6) (Schmidbauer et al., 2000; Zhou et al., 2011; Wang et al., 2012). Activation enthalpies obtained from our amphibole sample with 8.16 wt.% FeO at different pressure also fall within the range (0.79–0.83 eV). More importantly, it is found that there is a distinct negative dependence of Fe content on $\Delta H$ (i.e., higher Fe content tends to yield lower $\Delta H$) based on previous and present data both of before and after dehydrogenation. The relationship in amphibole

is similar to that in Fe-bearing nominally anhydrous minerals such as olivine and its high-pressure polymorphs (Yoshino et al., 2012) as well as orthopyroxene (Zhang and Yoshino, 2016), in which small polaron conduction dominates the bulk conductivity. Consequently, electron hopping (small polaron) between ferrous and ferric ions is suggested to dominate the bulk conductivity in Fe-bearing amphibole both before and after dehydrogenation.

The reaction of amphibole dehydrogenation produces $H_2$ rather than molecular water, and simultaneously accompanies the initial oxidation of $Fe^{2+}$, ultimately resulting in the formation of an oxy-amphibole component (Phillips et al., 1988),

$$Fe^{2+} + OH^- = Fe^{3+} + O^{2-} + \tfrac{1}{2}H_2. \quad (2)$$

Previous studies report that extensive dehydrogenation commonly occurs within a period of several hours (Hu et al., 2017; Manthilake et al., 2015; Sun et al., 2017). The process of $Fe^{2+}$ oxidation, however, is much slower and allows oxidation to continue even after complete dehydrogenation of sample in which the initial $Fe^{2+}$ content is greater than H content (Ungaretti, 1980). Our experiments also show that electrical conductivity reaches a steady value after keeping the sample at 873 K for more than three hours, which reflects the possibly complete dehydrogenation of sample. Additionally, the very slight variation of $\Delta H$ from ~0.80 eV before dehydrogenation, to ~0.70 eV after dehydrogenation, suggests that the conduction mechanism for charge transport remains unchanged during the two stages. Small polaron conduction continues to dominate the bulk conductivity after amphibole dehydrogenation even at temperatures above 873 K.

The modest increase in conductivity and weak decrease in $\Delta H$ after dehydrogenation is likely to be associated with an increase in $Fe^{3+}$ concentration due to the oxidation of $Fe^{2+}$, as well as structural adjustments. In the amphibole crystal structure, $Fe^{2+}$ may occupy all octahedral M sites with the predominant order pattern of M(3) > M(1) > M(2) > M(4) (Zema et al., 2012). Experiments on heat-treated amphibole show that $Fe^{2+}$ at the M(1) and M(3) sites oxidizes during the oxidation–dehydrogenation process, which produces $Fe^{3+}$ and one electron. Some $Fe^{2+}$ ions on the M(2) and M(4) sites exchange with Mg at the M(1) and M(3) sites and are then oxidized in a similar fashion (Ishida, 1998). As a consequence, the oxidation of $Fe^{2+}$ during dehydrogenation not only results in increased $Fe^{3+}$ content but also leads to a substantial decrease in bond strength at O(3), to which H predominantly bonds, that is compensated by shortening of the M(1)–O(3) and M(3)–O(3) bonds (Phillips et al., 1988). Accordingly, a decrease in the O(3) bond strength and M(1)–O(3) and M(3)–O(3) bond lengths leads to a decrease in the average $Fe^{3+}-Fe^{2+}$ distance, which ultimately reduces the energy required for electron hopping between $Fe^{2+}$ and $Fe^{3+}$ on M sites, analogous to ferromagnesian mantle minerals (Yoshino et al., 2012). The increase in conductivity and slight decrease in $\Delta H$ activation enthalpy after dehydrogenation are therefore attributed to increased $Fe^{3+}$ concentration and associated structural adjustments rather than a change of conduction mechanism.

### 4.2. Comparison with previous studies

In early period, the electrical conductivity of basic amphibolite saturated with saline fluids was reported at high temperature and high pressure by Glover and Vine (1994, 1995) using DC method. As shown in Fig. 7, the conductivity of amphibolite dominated by electrolyte is distinctly much higher than all of other data, however, the values gradually approach our results with increasing temperature, and even overlap with our data at highest temperature. It is likely that pore fluid in rock matrix progressively escaped with increasing temperature, and the intrinsic conduction

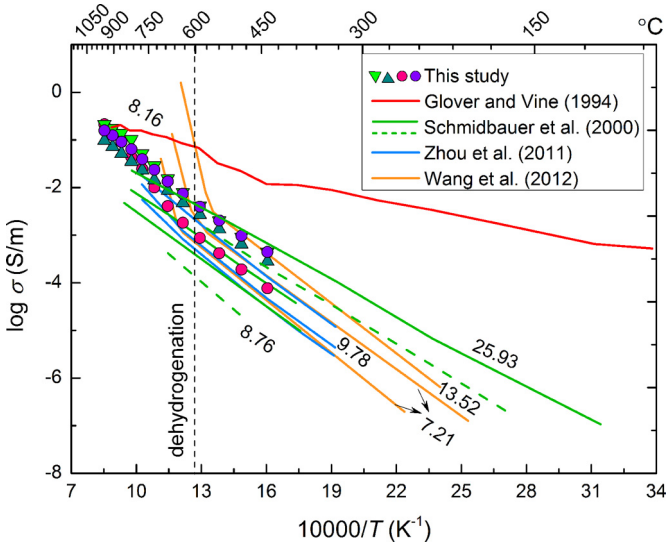


**Fig. 7.** Comparison of electrical conductivity of amphibole and amphibolite from present and previous studies. The numbers denote the total iron content (in wt.%) in samples. The red solid line denotes the result of amphibolite saturated with 0.5 M NaCl from Glover and Vine (1994). The green dotted and solid lines represent respectively the data of amphibole samples with different iron content before and after dehydrogenation from Schmidbauer et al. (2000). The blue and orange solid lines show the conductivity of amphibolite along different structural directions measured by Zhou et al. (2011) and Wang et al. (2012), respectively. Note that electrical conductivity seems to increase with increasing the total iron content in amphibole/amphibolite.

from major minerals (e.g., amphibole) began to play a role in the electrical conductivity of amphibolite. Thenceforth, with the application of AC impedance spectroscopy technique in geomaterials, the electrical conductivity of amphibole minerals were extensively measured by this method. Most conductivity experiments however were performed above the $T_D$ of amphibole, except for the data from Zhou et al. (2011), as indicated in Fig. 7. Based on these data, electrical conductivity appears to slightly increase with increasing Fe content prior to dehydrogenation. Our results are almost consistent with previous results from samples with similar Fe contents (Zhou et al., 2011; Wang et al., 2012). The effect of Fe concentration on the activation enthalpies (Fig. 6) and the electrical conductivity (Fig. 7) in amphibole/amphibolite further supports that small polaron conduction dominates the bulk conductivity, as total Fe content is an important controlling factor for hopping conduction (Yoshino et al., 2012). The discrepancies in conductivity reported in the literatures are therefore mainly attributed to the different Fe content in respective samples.

However, although the Fe content in amphibole from Schmidbauer et al. (2000) is a little higher (8.76 wt.%) than that in the present study (8.16 wt.%), they report conductivities about 0.5 log units lower than those found here, which may be due to the possible differences of $Fe^{3+}/\Sigma Fe$ between these samples. Another factor leading to differences between our data and previous results may be the anisotropy of electrical conductivity of amphibole. Zhou et al. (2011) and Wang et al. (2012) measured the conductivity of amphibolite along different structural directions under high $P$–$T$ conditions and reported an apparent conductivity anisotropy. Although the anisotropy of conductivity in amphibole was not measured in the present study, it is reasonable for our data to lie within previous conductivity values measured along different crystallographic axes.

The variation of conductivity and weak decrease of $\Delta H$ after dehydrogenation observed in this study are generally consistent with that reported by Schmidbauer et al. (2000), as shown in Fig. 7 and Fig. 6. In contrast, the conductivity values measured by Wang et al. (2012) increase abruptly when exceeding the sample

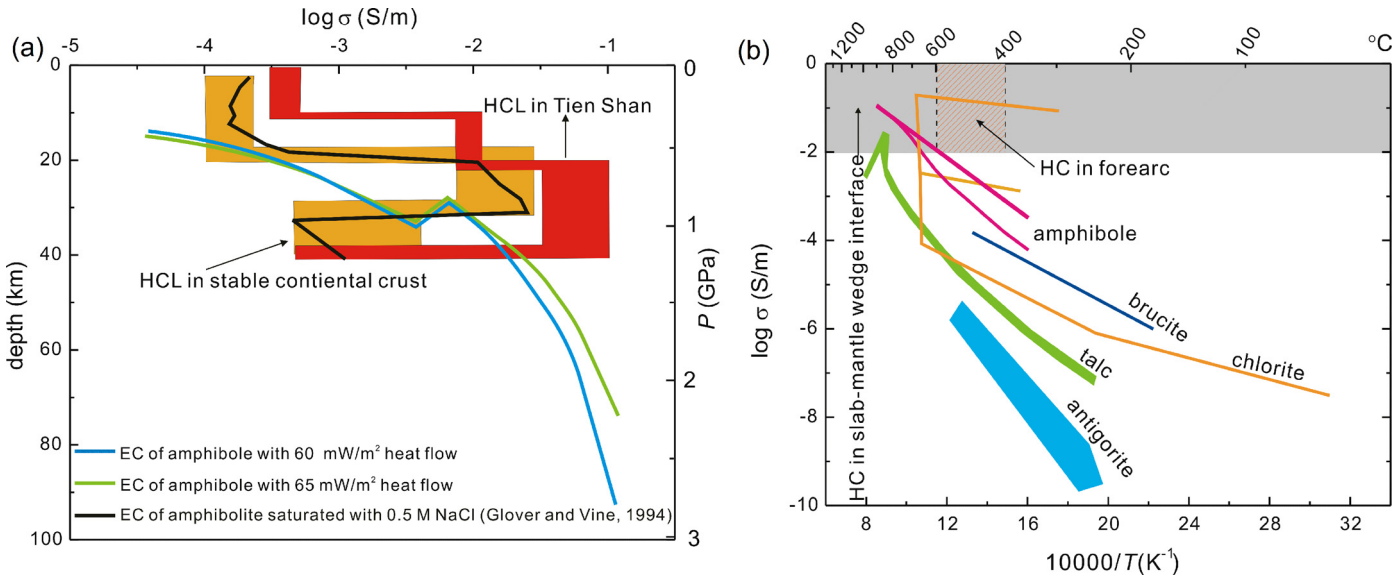


**Fig. 8.** (a) Comparison of laboratory-based conductivity profiles established from the present data of Fe-bearing amphibole with geophysically observed conductivity anomalies at depth of 20–40 km in stable continental mid-crust and Tien Shan. The blue and green lines represent the electrical conductivity (EC) profiles of amphibole based on average heat flows of 65 mW/m$^2$ in continental crust and 60 mW/m$^2$ in Tien Shan, respectively. The black line denotes the electrical conductivity profile of amphibolite saturated with 0.5 M NaCl from Glover and Vine (1994). (b) Comparison of laboratory-measured electrical conductivity of hydrous minerals with anomalous high conductivity ($10^{-2}$–1 S/m) in forearc area and slab–mantle wedge interface. The gray region corresponds to the high conductivity (HC) from geomagnetic observations. Data sources: Fe-bearing amphibole (this study), chlorite before and after dehydration (Manthilake et al., 2016), brucite perpendicular to the *c* axis at 3.7 GPa (Guo and Yoshino, 2014), antigorite (Reynard et al., 2011), talc aggregates (Wang and Karato, 2013). Abbreviation: HCL, high conductivity layer.

$T_D$ (above ~800 K), while $\Delta H$ the activation enthalpies values are anomalously large (up to 3.32–3.94 eV), far higher than those in Schmidbauer et al. (2000) and the present study (<1 eV). Wang et al. (2012) proposed that the high $\Delta H$ values may be related to a dehydration reaction associated with the oxidation–reduction reaction, however, they provided no further evidence to support this hypothesis. In addition, the conduction mechanism responsible for the anomalously high $\Delta H$ values was not identified. It is thus worth noting that caution should be taken when using these anomalously large conductivity data to interpret the high conductivity anomalies obtained from MT measurements.

### 4.3. Geophysical implications for highly conductive anomalies

#### 4.3.1. High conductivity in the continental crust

Experimental conductivity data combined with petrological models can provide independent and important constraints on the inversion results of MT soundings, which therefore improve our understanding of the Earth's interior (e.g., composition, structure, thermal state). We have constructed a conductivity–depth profile based on laboratory results of amphibole in this study and available geothermal data. Because high-conductivity anomalies are observed in both stable and tectonically active regions in the continental crust, and geothermal structures can vary significantly in different geotectonic environments, we adopt two sets of typical geothermal data from the stable continental crust (Pollack et al., 1993), and the Tien Shan (Vermeesch et al., 2004), corresponding to heat flows of 65 mW/m$^2$ and 60 mW/m$^2$, respectively. Conductivity as a function of depth were then constructed to compare directly with MT sounding results from the stable continental crust (Glover and Vine, 1994) and the Tien Shan region (Vanyan and Gliko, 1999). The effect of pressure on the conductivity–depth profile is neglected due to its very weak influence on the conductivity of amphibole determined from our data. In addition, the average pressure usually does not exceed 1.0 GPa at the base of Earth's crust.

As shown in Fig. 8a, an abrupt increase of conductivity at depths of ~35 km is displayed for both conductivity–depth profiles due to the oxidation–dehydrogenation of amphibole. For the stable continental crust, the amphibole conductivity–depth curve intersects the bottom of the highly conductive anomalies at approximately 30 km depth, that is, the conductivity of amphibole after oxidation–dehydrogenation almost reaches that of the high conductivity layers (HCLs) at the lowermost mid-crust where the value is about 0.01 S/m. Despite the conductivity of NaCl electrolyte saturated amphibolite from Glover and Vine (1994) can account for the MT observed mid-crustal conductivities, H-deficient amphibole formed by oxidation–dehydrogenation can provide an alternatively plausible explanation for the anomalously high conductivity observed in lowermost mid-crust of stable continent.

The mid-crustal conductivity anomaly in the Tien Shan is greater than that of stable continental crust while the heat flow is even lower than expected. Correspondingly, the conductivity–depth profile of amphibole is far below the HCL in the mid-crust beneath the Tien Shan, as shown in Fig. 8a. As a consequence, the enhanced conductivity of amphibole after oxidation–dehydrogenation can hardly account for the observed high conductivity anomaly in the Tien Shan. A previous study on the Tien Shan however attributed the HCL in the mid-crust to aqueous fluids released by dehydration of amphibole-bearing rocks occurring at 923–973 K (Vanyan and Gliko, 1999). Nevertheless, according to the present results, the dehydrogenation reaction would take place in amphibole at this temperature rather than dehydration, simultaneously producing hydrogen instead of water. The dehydrogenation reaction in amphibole at high temperature has also been extensively investigated in crystal chemical and petrological studies (Phillips et al., 1988; Zema et al., 2012; Della Ventura et al., 2017). Besides, the subsolidus decomposition of amphibole is reported to occur within the range of 1323–1373 K at 1 kbar, and the melting temperature is higher than 1398 K (Popp et al., 1995). Therefore, under the *P*–*T* conditions prevailing in the mid-crust of Tien Shan, amphibole dehydration is unlikely to occur during heating of the mid-crust and is furthermore impossible to provide a significant source of aqueous fluid. The electrical conductivity of 0.5 M NaCl electrolyte-saturated amphibolite rocks are also insufficient to explain the anomalously high conductivity observed in the mid-crust

beneath the Tien Shan. Aqueous fluids contain higher NaCl concentration from dehydration reaction of other hydrous minerals (Guo et al., 2015; Hyndman and Shearer, 1989) or other highly conductive materials, e.g., graphite films (Glover and Vine, 1992, 1995), Fe/Ti oxides or sulfides (Duba et al., 1994), partial melting (Glover et al., 2000) may therefore be required to account for the HCL in the mid-crust beneath Tien Shan. Nevertheless, in some tectonically active regions with anomalously high heat flow, e.g., Tibet Plateau, with 90 mW/m$^2$ (Hu et al., 2000), the MT observed high conductivity (Unsworth et al., 2005) is likely to be interpreted by the enhanced conductivity of dehydrogenated amphibole.

*4.3.2. High conductivity in subduction zones*

Electro-magnetic results from various subduction zones reveal a high conductivity anomaly in the forearc region at a depth of 10–40 km (Wannamaker et al., 2009; Worzewski et al., 2011; McGary et al., 2014; Pommier, 2014), which is usually interpreted as the presence of aqueous fluid released from the descending slab. Slab-derived $H_2O$ may migrate upwards and hydrate the upper-mantle peridotite in mantle wedge at shallow depths, thus generating large amounts of hydrous minerals including serpentine, talc, brucite, chlorite, and amphibole (Schmidt and Poli, 1998; Hyndman and Peacock, 2003). The temperature in forearc mantle is inferred to be below 873 K such that these hydrous minerals are stable in the forearc region where the physical properties (e.g., conductivity, seismic velocity) can be affected by these minerals. Previous experimental studies (Guo et al., 2011; Reynard et al., 2011; Wang and Karato, 2013) have shown that the conductivities of talc and serpentine is much lower than the high electrical conductors ($10^{-1}$–1 S/m) in forearc regions, as shown in Fig. 8b. Although the conductivity of chlorite shows a considerable increase after dehydration and subsequent enhancement of conductivity up to $7 \times 10^{-1}$ S/m (Manthilake et al., 2016), which is dominated by magnetite, the initial reaction occurs at 923 K (i.e., hotter than a cool forearc) and chlorite dehydration is therefore unlikely to occur. The presence of amphibole is also insufficient to explain highly conductive anomalies in forearc settings ($T < 873$ K), despite its high conductivity compared with other hydrous minerals. A saline aqueous fluid seems to be the best candidate for interpreting the global high conductivity anomalies in forearc areas even though the fluid volume fraction and salinity have not been given the uniform and accurate values from experiments (Sinmyo and Keppler, 2017) or simulation calculations (Sakuma and Ichiki, 2016) on the conductivity of NaCl–$H_2O$ fluid.

Another highly conductive zone also exists extensively at depths beyond 70 km; identified as the slab–mantle wedge interface from MT surveys (Wannamaker et al., 2009; Worzewski et al., 2011) where temperature usually exceeds 873 K (Currie and Hyndman, 2006). Worzewski et al. (2011) proposed the conductivity anomaly to be associated with de-serpentinization of the oceanic mantle, while the anomaly beneath New Zealand is attributed to fluids derived from amphibole–zoisite breakdown at 75–100 km depth near the subduction interface (Wannamaker et al., 2009). For the cool subduction zone in New Zealand, the dehydration of zoisite would take place at deeper depth (>100 km) based on the conductivity results of epidote/zoisite minerals (Hu et al., 2017). Petrological studies (Peacock, 1996; Ono, 1998) suggest that a hydrous layer composed of amphibole/chlorite-saturated peridotite exists at the base of the mantle wedge, formed from the dehydration of the underlying slab including subducting oceanic crust and serpentinized oceanic mantle. These hydrous phases are stable in peridotite up to 120 km depth, even deeper in cool subduction zones. Even if amphibole dehydrogenation and chlorite dehydration both occur due to the relatively high temperature at the slab–mantle wedge (>873 K), the enhanced conductivity of amphibole after dehydrogenation is comparable to that of chlorite after dehydration. The presence of H-deficient amphibole can therefore provide another reasonable explanation for high conductivity anomalies at the depths >70 km in the slab–mantle wedge interface.

The HCLs in the continental mid-crust, including the Tien Shan and subduction zones (e.g., forearc region, slab–mantle wedge interface), often present seismic wave attenuation anomalies (Roecker et al., 1993; Schurr et al., 2003; Chen and Clayton, 2009; Yang et al., 2012). Although seismic wave attenuation and Poisson's ratio are sensitive to the presence of fluid and temperature, a small amount of fluid fraction has only a rather small effect on seismic velocities (Ishikawa and Matsumoto, 2014), whereas it (e.g., 1 vol.% fluid with 5 wt.% NaCl) is sufficient to enhance the bulk conductivity to values that are expected in HCLs (Sinmyo and Keppler, 2017). In the forearc region, a large amount of fluid released from the subducting slab migrates upward by channel networks or deep fracture zones (Tauzin et al., 2017), resulting in the formation of fluid accumulation zones. Therefore, both high conductivity anomalies and low seismic velocities in the forearc region can be interpreted as the presence of a large quantity of slab-derived fluid. Nevertheless, aqueous fluid hardly seems to accumulate in comparable abundance in the continental mid-crust and slab–mantle wedge interface with that of the forearc regime. By contrast, elastic wave velocity data of amphibolite indicate both $V_p$ and $V_s$ gradually decrease with temperature and drop sharply around 923–973 K (Ito and Tatsumi, 1995), which sufficiently explains the low-velocity layer observed at the slab–mantle wedge interface where the velocity drop is ∼5%–6% compared with the surrounding rocks. Combining the enhanced conductivity of amphibole at similar temperature due to dehydrogenation in this study, the high conductivity and low velocity anomalies observed both in the lowermost continental mid-crust (particularly in localized regions with high heat flow) as well as the slab–mantle wedge interface are therefore likely due to the presence of dehydrogenated amphibole.

## 5. Conclusion

The influence of temperature on conductivity is much more pronounced than that of pressure. An abrupt change of impedance spectra and distinct enhancement of conductivity were observed around $843 \pm 20$ K. Post-experimental observations including optical and scanning electron microscopy, as well as FTIR analysis, demonstrate that these changes can be attributed to the oxidation–dehydrogenation reaction rather than dehydration-generated aqueous fluid. A slight variation of activation enthalpy from ∼0.80 eV before dehydrogenation to ∼0.70 eV after oxidation–dehydrogenation suggests that the conduction mechanism remains unchanged, and that small polaron conduction dominates amphibole conductivity, as further confirmed by the dependence of conductivity and activation enthalpy on Fe content of amphibole based on present and previous studies.

The laboratory-based conductivity–depth profile constructed from the amphibole conductivity data suggests that the presence of amphibole after dehydrogenation provides a reasonable explanation for the high conductivity anomalies in the continental lowermost mid-crust, particularly in some local regions with high heat flow. In contrast, the greater conductivity anomaly in the mid-crust of the Tien Shan is insufficient to be explained by H-deficient amphibole, although its conductivity is enhanced after oxidation–dehydrogenation. Moreover, the anomalous high conductivity of $>10^{-2}$ S/m observed in the slab–mantle wedge interface at depth >70 km where temperature is usually higher than 873 K, can be likely interpreted by the presence of dehydrogenated amphibole, whereas large amounts of slab-derived aqueous fluid may be the origin of the high conductivity anomalies in the forearc areas at

20–40 km depth. In combination with previous elastic wave velocity data, amphibole after dehydrogenation can simultaneously be responsible for the high conductivity and low velocity anomalies observed in both the lowermost mid-crust of stable continent and slab–mantle wedge interface.

## Acknowledgements

The authors are grateful to Duojun Wang for technical assistance regarding conductivity measurement experiments and Nao Cai for operation of the multi-anvil apparatus at the MPI of Stony Brook University. We also thank Shaohua Dong and Wenqing Zheng for their help with SEM and electron microprobe analyses. This study was financially supported by the Strategic Priority Research Program (B) of the Chinese Academy of Sciences (XDB 18010401), Key Research Program of Frontier Sciences of CAS (QYZDB-SSW-DQC009), "135" Program of the Institute of Geochemistry of CAS, Hundred Talents Program of CAS and NSF of China (41772042, 41474078 and 41774099), and the Chinese Scholarship Council (201504910202). Baosheng Li acknowledges support from the DOE/NNSA (Grant No. DE-NA0002907) and the National Science Foundation (Grant No. EAR1524078). We thank Esther Posner, PhD, for editorial assistance.

## Appendix A. Supplementary material

Supplementary material related to this article can be found online at https://doi.org/10.1016/j.epsl.2018.06.003.

## References

Chen, S., Guo, X., Yoshino, T., Jin, Z., Li, P., 2017. Dehydration of phengite inferred by electrical conductivity measurements: implication for the high conductivity anomalies relevant to the subduction zones. Geology 46, 11–14.

Chen, T., Clayton, R.W., 2009. Seismic attenuation structure in central Mexico: image of a focused high-attenuation zone in the mantle wedge. J. Geophys. Res., Solid Earth 114, B07034. https://doi.org/10.1029/2008JB005964.

Christensen, N.I., Mooney, W.D., 1995. Seismic velocity structure and composition of the continental crust: a global view. J. Geophys. Res., Solid Earth 100, 9761–9788.

Currie, C.A., Hyndman, R.D., 2006. The thermal structure of subduction zone back arcs. J. Geophys. Res., Solid Earth 111, B08404. https://doi.org/10.1029/2005JB004024.

Dai, L., Hu, H., Li, H., Wu, L., Hui, K., Jiang, J., Sun, W., 2016. Influence of temperature, pressure, and oxygen fugacity on the electrical conductivity of dry eclogite, and geophysical implications. Geochem. Geophys. Geosyst. 17, 2394–2407. https://doi.org/10.1002/2016GC006282.

Della Ventura, G., Susta, U., Bellatreccia, F., Marcelli, A., Redhammer, G.J., 2017. Deprotonation of Fe-dominant amphiboles: single-crystal HT-FTIR spectroscopic studies of synthetic potassic-ferro-richterite. Am. Mineral. 102, 117–125.

Duba, A., Heikamp, S., Meurer, W., Mover, G., Will, G., 1994. Evidence from borehole samples for the role of accessory minerals in lower-crustal conductivity. Nature 367, 59–61.

Evans, R.L., Wannamaker, P.E., McGary, R.S., Elsenbeck, J., 2014. Electrical structure of the central Cascadia subduction zone: the EMSLAB Lincoln Line revisited. Earth Planet. Sci. Lett. 402, 265–274.

Glover, P., Vine, F., 1992. Electrical conductivity of carbon-bearing granulite at raised temperatures and pressures. Nature 360, 723–726.

Glover, P.W., Vine, F., 1994. Electrical conductivity of the continental crust. Geophys. Res. Lett. 21, 2357–2360.

Glover, P.W.J., Vine, F.J., 1995. Beyond KTB-electrical conductivity of the deep continental crust. Surv. Geophys. 16, 5–36.

Glover, P.W.J., Pous, J., Queralt, P., Muñoz, J.-A., Liesa, M., Hole, M.J., 2000. Integrated two-dimensional lithospheric conductivity modelling in the Pyrenees using field-scale and laboratory measurements. Earth Planet. Sci. Lett. 178, 59–72.

Guo, X., Yoshino, T., Katayama, I., 2011. Electrical conductivity anisotropy of deformed talc rocks and serpentinites at 3 GPa. Phys. Earth Planet. Inter. 188, 69–81.

Guo, X., Yoshino, T., 2014. Pressure-induced enhancement of proton conduction in brucite. Geophys. Res. Lett. 41, 813–819.

Guo, X., Yoshino, T., Shimojuku, A., 2015. Electrical conductivity of albite–(quartz)–water and albite–water–NaCl systems and its implication to the high conductivity anomalies in the continental crust. Earth Planet. Sci. Lett. 412, 1–9.

Hicks, T.L., Secco, R.A., 1997. Dehydration and decomposition of pyrophyllite at high pressures: electrical conductivity and X-ray diffraction studies to 5 GPa. Can. J. Earth Sci. 34, 875–882.

Hu, H., Dai, L., Li, H., Hui, K., Sun, W., 2017. Influence of dehydration on the electrical conductivity of epidote and implications for high-conductivity anomalies in subduction zones. J. Geophys. Res., Solid Earth 122, 2751–2762.

Hu, S., He, L., Wang, J., 2000. Heat flow in the continental area of China: a new data set. Earth Planet. Sci. Lett. 179, 407–419.

Hyndman, R., Shearer, P., 1989. Water in the lower continental crust: modelling magnetotelluric and seismic reflection results. Geophys. J. Int. 98, 343–365.

Hyndman, R.D., Peacock, S.M., 2003. Serpentinization of the forearc mantle. Earth Planet. Sci. Lett. 212, 417–432.

Ishida, K., 1998. Cation disordering in heat-treated anthophyllites through oxidation and dehydrogenation. Phys. Chem. Miner. 25, 160–167.

Ishikawa, M., Matsumoto, Y., 2014. Effect of fluid $H_2O$ on compressional wave velocities in quartz aggregate up to 500 °C at 0.5 GPa. Earth Planets Space 66, 35. https://doi.org/10.1186/1880-5981-66-35.

Ito, K., Tatsumi, Y., 1995. Measurement of elastic wave velocities in granulite and amphibolite having identical $H_2O$-free bulk compositions up to 850 °C at 1 GPa. Earth Planet. Sci. Lett. 133, 255–264.

Kawano, S., Yoshino, T., Katayama, I., 2012. Electrical conductivity of magnetite-bearing serpentinite during shear deformation. Geophys. Res. Lett. 39, L20313. https://doi.org/10.1029/2012GL053652.

Leibecker, J., Gatzemeier, A., Honig, M., Kuras, O., Soyer, W., 2002. Evidence of electrical anisotropic structures in the lower crust and the upper mantle beneath the Rhenish Shield. Earth Planet. Sci. Lett. 202, 289–302.

Macdonald, D.D., 1978. A method for estimating impedance parameters for electrochemical systems that exhibit pseudoinductance. J. Electrochem. Soc. 125, 2062–2064.

Manthilake, G., Mookherjee, M., Bolfan-Casanova, N., Andrault, D., 2015. Electrical conductivity of lawsonite and dehydrating fluids at high pressures and temperatures. Geophys. Res. Lett. 42, 7398–7405.

Manthilake, G., Bolfan-Casanova, N., Novella, D., Mookherjee, M., Andrault, D., 2016. Dehydration of chlorite explains anomalously high electrical conductivity in the mantle wedges. Sci. Adv. 2, e1501631. https://doi.org/10.1126/sciadv.1501631.

McCammon, C., Frost, D., Smyth, J., Laustsen, H., Kawamoto, T., Ross, N., Van Aken, P., 2004. Oxidation state of iron in hydrous mantle phases: implications for subduction and mantle oxygen fugacity. Phys. Earth Planet. Inter. 143, 157–169.

McGary, R.S., Evans, R.L., Wannamaker, P.E., Elsenbeck, J., Rondenay, S., 2014. Pathway from subducting slab to surface for melt and fluids beneath Mount Rainier. Nature 511, 338–340.

Ono, S., 1998. Stability limits of hydrous minerals in sediment and mid-ocean ridge basalt compositions: implications for water transport in subduction zones. J. Geophys. Res., Solid Earth 103, 18253–18267.

Peacock, S.M., 1996. Thermal and petrologic structure of subduction zones. In: Bebout, G., Scholl, D.W., Kirby, S.H., Platt, J.P. (Eds.), Subduction: Top to Bottom. In: Geophysical Monographs, vol. 96. Am. Geophys. Union, Washington, DC, pp. 119–133.

Phillips, M., Popp, R., Clowe, C., 1988. Structural adjustments accompanying oxidation–dehydrogenation in amphiboles. Am. Mineral. 73, 500–506.

Pollack, H.N., Hurter, S.J., Johnson, J.R., 1993. Heat flow from the Earth's interior: analysis of the global data set. Rev. Geophys. 31, 267–280.

Pommier, A., 2014. Geophysical assessment of migration and storage conditions of fluids in subduction zones. Earth Planets Space 66, 38. https://doi.org/10.1186/1880-5981-66-38.

Popp, R.K., Virgo, D., Yoder, H.S., Hoering, T.C., Phillips, M.W., 1995. An experimental study of phase equilibria and Fe oxy-component in kaersutitic amphibole, implications for the $f_{H_2}$ and $a_{H_2O}$ in the upper mantle. Am. Mineral. 80, 534–548.

Reynard, B., Mibe, K., de Moortèle, B.V., 2011. Electrical conductivity of the serpentinised mantle and fluid flow in subduction zones. Earth Planet. Sci. Lett. 307, 387–394.

Roberts, J.J., Tyburczy, J.A., 1991. Frequency dependent electrical properties of polycrystalline olivine compacts. J. Geophys. Res., Solid Earth 96, 16205–16222.

Roecker, S., Sabitova, T., Vinnik, L., Burmakov, Y.A., Golvanov, M., Mamatkanova, R., Munirova, L., 1993. Three-dimensional elastic wave velocity structure of the western and central Tien Shan. J. Geophys. Res., Solid Earth 98, 15779–15795.

Sakuma, H., Ichiki, M., 2016. Electrical conductivity of NaCl–$H_2O$ fluid in the crust. J. Geophys. Res., Solid Earth 121, 577–594. https://doi.org/10.1002/2015JB012219.

Schilling, F.R., Partzsch, G.M., Brasse, H., Schwarz, G., 1997. Partial melting below the magmatic arc in the central Andes deduced from geoelectromagnetic field experiments and laboratory data. Phys. Earth Planet. Inter. 103, 17–31.

Schmidbauer, E., Kunzmann, T., Fehr, T., Hochleitner, R., 2000. Electrical resistivity and 57 Fe Mössbauer spectra of Fe-bearing calcic amphiboles. Phys. Chem. Miner. 27, 347–356.

Schmidt, M.W., Poli, S., 1998. Experimentally based water budgets for dehydrating slabs and consequences for arc magma generation. Earth Planet. Sci. Lett. 163, 361–379.

Schurr, B., Asch, G., Rietbrock, A., Trumbull, R., Haberland, C., 2003. Complex patterns of fluid and melt transport in the central Andean subduction zone revealed by attenuation tomography. Earth Planet. Sci. Lett. 215, 105–119.

Shan, S., Wang, R., Guo, J., Li, H., 2007. Pressure calibration for the sample cell of YJ-3000t multi-anvil press at high-temperature and high-pressure. Chin. J. High Press. Phys. 21, 367–372 (in Chinese).

Sinmyo, R., Keppler, H., 2017. Electrical conductivity of NaCl-bearing aqueous fluids to 600 °C and 1 GPa. Contrib. Mineral. Petrol. 172, 4. https://doi.org/10.1007/s00410-016-1323-z.

Sun, W., Dai, L., Li, H., Hu, H., Wu, L., Jiang, J., 2017. Electrical conductivity of mudstone (before and after dehydration at high P–T) and a test of high conductivity layers in the crust. Am. Mineral. 102, 2450–2456.

Tauzin, B., Reynard, B., Perrillat, J.-P., Debayle, E., Bodin, T., 2017. Deep crustal fracture zones control fluid escape and the seismic cycle in the Cascadia subduction zone. Earth Planet. Sci. Lett. 460, 1–11.

Tolland, H., 1973. Mantle conductivity and electrical properties of garnet, mica and amphibole. Nature 241, 35–36.

Ungaretti, L., 1980. Recent developments in X-ray single crystal diffractometry applied to the crystal-chemical study of amphiboles. God. Jugosl. Cent. Krist. 15, 29–65.

Unsworth, M., Jones, A.G., Wei, W., Marquis, G., Gokarn, S., Spratt, J., Bedrosian, P., Booker, J., Leshou, C., Clarke, G., 2005. Crustal rheology of the Himalaya and Southern Tibet inferred from magnetotelluric data. Nature 438, 78–81.

Vanyan, L.L., Gliko, A.O., 1999. Seismic and electromagnetic evidence of dehydration as a free water source in the reactivated crust. Geophys. J. Int. 137, 159–162.

Vermeesch, P.J., Poort, A.D., Duchkov, J.K., Batist, M.D., 2004. Lake Issyk-Kul (Tien Shan): unusually low heat flow in an active intermontane basin. Geol. Geofiz. 45, 616–625.

Wang, D., Guo, Y., Yu, Y., Karato, S., 2012. Electrical conductivity of amphibole-bearing rocks: influence of dehydration. Contrib. Mineral. Petrol. 164, 17–25.

Wang, D., Karato, S., 2013. Electrical conductivity of talc aggregates at 0.5 GPa: influence of dehydration. Phys. Chem. Miner. 40, 11–17.

Wannamaker, P.E., Caldwell, T.G., Jiracek, G.R., Maris, V., Hill, G.J., Ogawa, Y., Bibby, H.M., Bennie, S.L., Heise, W., 2009. Fluid and deformation regime of an advancing subduction system at Marlborough, New Zealand. Nature 460, 733–736.

Worzewski, T., Jegen, M., Kopp, H., Brasse, H., Castillo, W.T., 2011. Magnetotelluric image of the fluid cycle in the Costa Rican subduction zone. Nat. Geosci. 4, 108–111.

Yang, Y., Ritzwoller, M.H., Zheng, Y., Shen, W., Levshin, A.L., Xie, Z., 2012. A synoptic view of the distribution and connectivity of the mid-crustal low velocity zone beneath Tibet. J. Geophys. Res., Solid Earth 117, B04303. https://doi.org/10.1029/2011JB008810.

Yoshino, T., Shimojuku, A., Shan, S., Guo, X., Yamazaki, D., Ito, E., Higo, Y., Funakoshi, K., 2012. Effect of temperature, pressure and iron content on the electrical conductivity of olivine and its high-pressure polymorphs. J. Geophys. Res., Solid Earth 117, B08205. https://doi.org/10.1029/2011JB008774.

Zema, M., Welch, M.D., Oberti, R., 2012. High-T behaviour of gedrite: thermoelasticity, cation ordering and dehydrogenation. Contrib. Mineral. Petrol. 163, 923–937.

Zhang, B., Yoshino, T., 2016. Effect of temperature, pressure and iron content on the electrical conductivity of orthopyroxene. Contrib. Mineral. Petrol. 171, 102. https://doi.org/10.1007/s00410-016-1315-z.

Zhou, W., Fan, D., Liu, Y., Xie, H., 2011. Measurements of wave velocity and electrical conductivity of an amphibolite from southwestern margin of the Tarim Basin at pressures to 1.0 GPa and temperatures to 700 °C: comparison with field observations. Geophys. J. Int. 187, 1393–1404.